




---

# Measurement of Trilinear Gauge Boson Couplings $WWV$ ( $V \equiv Z, \gamma$ ) in $e^+e^-$ Collisions at 189 GeV

Preliminary results for the ICHEP 2000 conference

**T.J.V. Bowcock**<sup>1</sup>, **C. DeClercq**<sup>2</sup>, **G. Fanourakis**<sup>3</sup>, **D. Fassouliotis**<sup>3</sup>, **D. Gelé**<sup>4</sup>,  
**B. Golob**<sup>5</sup>, **B. Kersevan**<sup>5</sup>, **A. Kinvig**<sup>1</sup>, **V. Kostioukhine**<sup>6</sup>, **J. Libby**<sup>7</sup>, **A. Leisos**<sup>3</sup>,  
**N. Mastroyiannopoulos**<sup>3</sup>, **C. Matteuzzi**<sup>8</sup>, **M. McCubbin**<sup>1</sup>, **M. Nassiakou**<sup>3</sup>,  
**G. Orazi**<sup>4</sup>, **U. Parzefall**<sup>1</sup>, **H.T. Phillips**<sup>9</sup>, **R.L. Sekulin**<sup>9</sup>, **F. Terranova**<sup>8</sup>,  
**M. Tobin**<sup>1</sup>, **S. Tzamarias**<sup>3</sup>, **A. Van Lysebetten**<sup>2</sup>, **O. Yushchenko**<sup>6</sup>

<sup>1</sup> Department of Physics, University of Liverpool, P.O. Box 147, Liverpool L69 3BX, UK

<sup>2</sup> IIHE-Institut Universitaire des Hautes Energies, Pleinlaan 2, B-1050 Brussels, Belgium

<sup>3</sup> Institute of Nuclear Physics, N.C.S.R. Demokritos, P.O. Box 60228, GR-15310 Athens, Greece

<sup>4</sup> Institut de Recherches Subatomiques, B.P. 20 CRO, F-67037 Strasbourg Cedex, France

<sup>5</sup> Univerza v Ljubljani, Institut Josef Stefan, Jamova 39, P.O.B 3000, SI-1001 Ljubljana, Slovenia

<sup>6</sup> Inst. for High Energy Physics, Serpukhov P.O. Box 35, Protvino, (Moscow Region), Russian Federation

<sup>7</sup> Department of Physics, University of Oxford, Keble Road, Oxford OX1 3RH, UK

<sup>8</sup> Dipartimento di Fisica, Università di Milano and INFN, Via Celoria 16, I-20133 Milan, Italy

<sup>9</sup> Rutherford Appleton Laboratory, Chilton, Didcot OX11 OQX, UK

## Abstract

Measurements of the trilinear gauge boson couplings  $WW\gamma$  and  $WWZ$  are presented from data taken by DELPHI in 1998 at a centre-of-mass energy of 189 GeV and combined with available DELPHI data at lower energies. Values are determined for  $\Delta g_1^Z$  and  $\Delta\kappa_\gamma$ , the differences of the  $WWZ$  charge coupling and of the  $WW\gamma$  dipole coupling from their Standard Model values, and for  $\lambda_\gamma$ , the  $WW\gamma$  quadrupole coupling. A measurement of the magnetic dipole and electric quadrupole moment of the W is extracted from the results for  $\Delta\kappa_\gamma$  and  $\lambda_\gamma$ . The study uses data from the final states  $jj\ell\nu$ ,  $jjjj$ ,  $\ell X$ ,  $jjX$  and  $\gamma X$ , where  $j$  represents a quark jet,  $\ell$  an identified lepton and  $X$  missing four-momentum. The observations are consistent with the predictions of the Standard Model.

# 1 Introduction

The properties of the final state in the reactions  $e^+e^- \rightarrow W^+W^-$ ,  $W\nu\bar{\nu}$  and  $\nu\nu\gamma$  are sensitive to trilinear gauge boson couplings [1, 2]. This study uses data from the final states  $jj\ell\nu$ ,  $jjjj$ ,  $\ell^+\ell^-X$ ,  $\ell X$ ,  $jjX$  and  $\gamma X$  (where  $j$  represents a quark jet,  $\ell$  an identified lepton and  $X$  missing four-momentum) taken by the DELPHI detector at LEP in 1998 at a centre-of-mass energy of 189 GeV. The data are used to determine values of three coupling parameters at the  $WWV$  vertex (with  $V \equiv \gamma, Z$ ):  $\Delta g_1^Z$ , the difference between the value of the overall  $WWZ$  coupling strength and its Standard Model prediction;  $\Delta\kappa_\gamma$ , the difference between the value of the dipole coupling,  $\kappa_\gamma$ , and its Standard Model value; and  $\lambda_\gamma$ , the  $WW\gamma$  quadrupole coupling parameter [3].

In the evaluation of the couplings, a model has been assumed [4] in which contributions to the effective  $WWV$  Lagrangian from operators describing possible new physics beyond the Standard Model are restricted to those which are  $CP$ -conserving, are of lowest dimension ( $\leq 6$ ), satisfy  $SU(2) \times U(1)$  invariance, and have not been excluded by previous measurements. This leads to possible contributions from three operators,  $\mathcal{L}_{W\phi}$ ,  $\mathcal{L}_{B\phi}$  and  $\mathcal{L}_W$ , and hence to relations between the permitted values of the  $WW\gamma$  and  $WWZ$  couplings:  $\Delta\kappa_Z = \Delta g_1^Z - \frac{s_w^2}{c_w^2} \Delta\kappa_\gamma$ , and  $\lambda_Z = \lambda_\gamma$ , where  $s_w$  and  $c_w$  are the sine and cosine of the electroweak mixing angle. The parameters we determine are related to possible contributions  $\alpha_{W\phi}$ ,  $\alpha_{B\phi}$  and  $\alpha_W$  from the three operators given above by:  $\Delta g_1^Z = \alpha_{W\phi}/c_w^2$ ,  $\Delta\kappa_\gamma = \alpha_{W\phi} + \alpha_{B\phi}$ , and  $\lambda_\gamma = \alpha_W$ .

The  $WWV$  coupling arises in  $WW$  production through the diagrams involving  $s$ -channel exchange of  $Z$  or  $\gamma$ , shown in figure 1a. We study this reaction in the final states  $jj\ell\nu$ , where one  $W$  decays into quarks and the other into leptons, and  $jjjj$ , where both  $W$ s decay into quarks.

In single  $W$  production, the dominant amplitude involving a trilinear gauge coupling arises from the radiation of a virtual photon from the incident electron or positron, interacting with a virtual  $W$  radiated from the other incident particle (figure 1b). This process, involving a  $WW\gamma$  coupling, contributes significantly in the kinematic region where a final state electron or positron is emitted at small angle to the beam and is thus likely to remain undetected in the beam pipe. The decay modes of the  $W$  give rise to two final states: that with two jets and missing energy ( $jjX$ ), and that containing only a single visible lepton coming from the interaction point and no other track in the detector ( $\ell X$ ).

The trilinear  $WW\gamma$  vertex also occurs in the reaction  $e^+e^- \rightarrow \nu\nu\gamma$  in the diagram in which the incoming electron and positron each radiate a virtual  $W$  at an  $e\nu W$  vertex and these two fuse to produce an outgoing photon (figure 1c). In this process, which leads to a final state,  $\gamma X$ , consisting of a single detected photon, the  $WW\gamma$  coupling is studied completely independently of the  $WWZ$  coupling, as no  $WWZ$  vertex is involved.

The next section of this paper describes the selection of events from the data and the simulation of the various channels involved in the analysis, and section 3 describes the methods used in the determination of coupling parameters. In section 4 the results from different channels are presented and combined with previously published DELPHI results [1, 2] to give overall values for the coupling parameters. A summary is given in section 5.

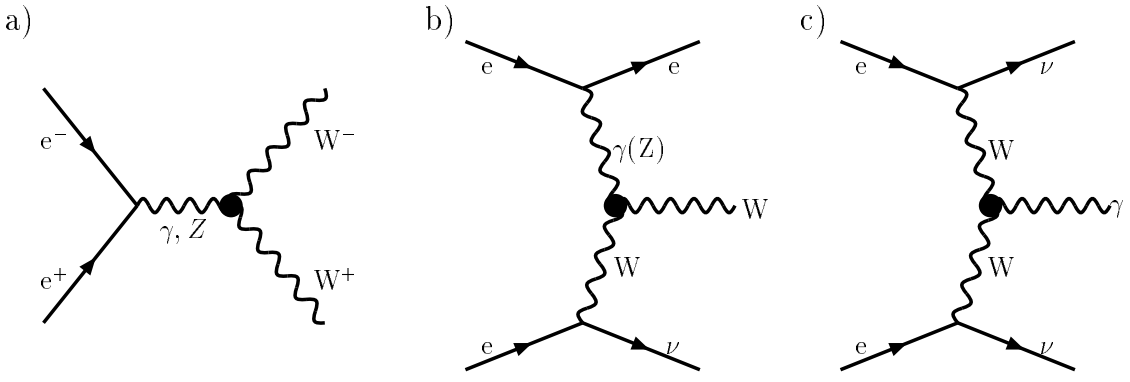


Figure 1: Diagrams with trilinear gauge boson couplings contributing to the processes studied in this paper: a)  $e^+e^- \rightarrow W^+W^-$ , b)  $e^+e^- \rightarrow We\nu$ , c)  $e^+e^- \rightarrow \nu\nu\gamma$ .

## 2 Event simulation and selection

In 1998 DELPHI recorded a total integrated luminosity of  $155 \text{ pb}^{-1}$  at an average centre-of-mass energy of  $188.63 \pm 0.04 \text{ GeV}$ . We describe here the main features of the selection of events in the final state topologies  $jj\ell\nu$ ,  $jjjj$ ,  $\ell X$ ,  $jjX$  and  $\gamma X$ , defined in the previous section. A detailed description of the DELPHI detector may be found in [5], which includes descriptions of the main components of the detector used in this study, namely, the trigger system, the luminosity monitor, the tracking system in the barrel and forward regions, the muon detectors, the electromagnetic calorimeters and the hermeticity counters. The definition of the criteria imposed for track selection and lepton identification and a description of the luminosity measurement are described in [6].

### Event simulation:

Various Monte Carlo models were used in the calculation of cross-sections as a function of coupling parameters in the different final states analysed. In the study of the  $jj\ell\nu$  and  $jjjj$  channels, the four-fermion generators EXCALIBUR [7] and ERATO [8] were used; the studies of the  $\ell X$  and  $jjX$  final states used calculations based on the program DELTGC [9], cross-checked with GRC4F [10]; DELTGC and NUNUGPV [11] were used to calculate the signals expected in the  $\gamma X$  topology. The EXCALIBUR and GRC4F models were interfaced to the JETSET hadronization model [12] tuned to  $Z$  data [13]. The study of backgrounds due to  $q\bar{q}(\gamma)$  production was made using events from the PYTHIA model [14], while EXCALIBUR was used to study the  $q\bar{q}\nu\bar{\nu}$  contribution to the  $jjX$  topology, and KORALZ [15], BHWIDE [16] and TEEG [17] were used in the calculation of backgrounds in the  $\ell X$  final state. PYTHIA and EXCALIBUR were used in the simulation of events from  $ZZ$  production. Two-photon backgrounds were studied using the generators of Berends, Daverveldt and Kleiss [18] and the TWOGAM generator [19]. All of the mentioned generators are interfaced to the full DELPHI simulation program [5], apart from DELTGC and ERATO which are used only to calculate event weights as a function of trilinear gauge coupling parameter values.

### Selection of events in the $jj\ell\nu$ topology:

Events in the  $jj\ell\nu$  topology are characterised by two hadronic jets, a lepton and missing momentum resulting from the neutrino. The lepton may be an electron or muon (coming either from  $W$  decay or from the cascade decay  $W \rightarrow \tau \dots \rightarrow \ell \dots$ ) or, in the case of  $\tau$  decays, the  $\tau$  might give rise to a low multiplicity jet. The major backgrounds come from  $q\bar{q}(\gamma)$  production and from four-fermion final states containing two quarks and two leptons of the same flavour.

Events with several hadrons were selected by requiring 5 or more charged particles and a total energy of charged particles recorded in the detector exceeding 15% of the centre-of-mass energy. In the selection of  $jj\mu\nu$  and  $jje\nu$  events, the candidate lepton was assumed to be the most energetic charged particle in the event; for  $jj\tau\nu$  events, the lepton candidates were constructed by looking for an isolated  $e$  or  $\mu$  or a low multiplicity jet.

The selection procedure was identical to that used in our analysis of data at 183 GeV [2], except that, in the selection of electron candidates, the component of the missing momentum transverse to the beam axis was required to be greater than 15 GeV/ $c$  and the angle between the candidate and the missing momentum was required to exceed 60°.

The efficiency for the selection of  $jj\ell\nu$  events was evaluated using fully simulated events to be  $(79.3 \pm 0.2)\%$ ,  $(59.4 \pm 0.3)\%$  and  $(31.7 \pm 0.3)\%$  for muon, electron and tau events, respectively. Using data taken only when all essential components of the detector were operational, corresponding to an integrated luminosity of 149 pb $^{-1}$ , 263 muon, 212 electron and 146 tau candidate events were selected. A background contamination of  $(0.226 \pm 0.016)$  pb was estimated, of which 58% came from the  $q\bar{q}(\gamma)$  final state, 22% from  $Z e^+ e^-$ , 13% from  $ZZ$  and  $Z\gamma^*$  production, and small contributions from non-semileptonic  $WW$  events and other sources. The errors on the efficiencies and background contributions (where given) are derived from simulation statistics for all channels analysed. The systematic uncertainty resulting from these statistical errors is included in our results shown in section 4.

### Selection of events in the $jjjj$ topology:

The selection of events in the fully hadronic topology followed closely that used in our analysis of data at 183 GeV [2], with only small changes in the values of kinematic cuts.

All detected particles were first clustered into jets using LUCLUS with  $d_{join} = 5.5$  GeV/ $c$ . Events were accepted if they had at least four jets, with at least four particles per jet. Background from  $Z\gamma$  events was suppressed by imposing the condition  $\sqrt{s'} > 130$  GeV, where  $\sqrt{s'}$  is an estimate of the effective collision energy in the (background)  $q\bar{q}(\gamma)$  final state after initial state radiation [20]. Events were then forced into a 4-jet configuration and a 4-constraint fit was performed, requiring conservation of four-momentum. Then, in order to suppress the dominant background, which arises from the  $q\bar{q}\gamma$  final state, the condition  $D > 0.0055$  GeV $^{-1}$  was imposed, with  $D = \frac{E_{min}}{E_{max}}\theta_{min}/(E_{max} - E_{min})$ ;  $E_{min}$  and  $E_{max}$  are the energies of the reconstructed jets with minimum and maximum energy and  $\theta_{min}$  is the minimum interjet angle. A further fit was then performed on surviving events, imposing four-momentum conservation and requiring the masses of the two reconstructed  $W$ s to be equal. The fit was applied to all three possible pairings of the four jets into two  $W$ s. Fits with reconstructed  $W$  mass outside the range  $74 < m_W^{rec} < 88$  GeV/ $c^2$  were rejected and, of the remaining fits, the

one with minimum  $\chi^2$  was accepted.

The efficiency of the selection procedure was evaluated from fully simulated events to be  $(75.7 \pm 0.2)\%$ . A total of 1130 events was selected from data corresponding to the full integrated luminosity of  $155 \text{ pb}^{-1}$ . Background contributions of  $(1.26 \pm 0.02) \text{ pb}$  and  $(0.187 \pm 0.007) \text{ pb}$  were estimated from  $q\bar{q}\gamma$  and  $jj\ell\nu$  production, respectively. The method used in the analysis of the data to assign the reconstructed jets to  $W$  pairs was applied to a sample of simulated events generated with only the three doubly resonant diagrams for  $WW$  production present in the production amplitude; in this model the efficiency of the procedure was estimated to be about 74%.

An additional problem in the analysis of the  $jjjj$  state is to distinguish the pair of jets constituting the  $W^+$  decay products from that from the  $W^-$ . This ambiguity can be partly resolved by computing jet charges from the momentum-weighted charge of each particle belonging to the jet,  $Q_{jet} = \sum_i q_i |p_i|^{0.5} / \sum_i |p_i|^{0.5}$  (where  $q_i$  and  $p_i$  are the charge and the momentum of the particle and the exponent is chosen empirically), and defining the  $W^\pm$  charges,  $Q_{W^+}$  and  $Q_{W^-}$ , as the sums of the charges of the two daughter jets. Following the method of [21], the distribution of the difference  $\Delta Q = Q_{W^-} - Q_{W^+}$  was then used to construct an estimator  $P_{W^-}(\Delta Q)$  of the probability that the pair with the more negative value of  $Q_W$  is a  $W^-$ . An estimate of the efficiency of this procedure was made by flagging all correctly associated jet pairs reconstructed from simulated events with  $\Delta Q < 0$  as  $W^-$  and comparing with the generated information: a value of 77% was obtained.

### Selection of events in the $\ell X$ topology:

In the selection of candidates for the  $\ell X$  final state, events were required to have only one charged particle, clearly identified as a muon from the signals recorded in the barrel or forward muon chambers or as an electron from the signals in the barrel or forward electromagnetic calorimeters. The corresponding selection criteria are described in detail in [6]. In addition, the normal track selections were tightened: the track was required to pass within 1 mm of the interaction point in the  $xy$  plane (perpendicular to the beam) and within 4 cm in  $z$ . Lepton candidates were also required to have momentum below  $75 \text{ GeV}/c$ , with a component transverse to the beam above  $20 \text{ GeV}/c$ . Events were rejected if there was an energy deposition of more than 5 GeV in the barrel or forward electromagnetic calorimeters which was not associated with one of the charged particle tracks, or if there was any signal in the hermeticity detectors. In the selection of electron candidates, the ratio of the energy measured in the electromagnetic calorimeter to the magnitude of the measured momentum was required to exceed 0.7.

Imposing these criteria, an efficiency of  $(31.2 \pm 3.8)\%$  was obtained in the  $eX$  channel for  $ee\nu\nu$  production, and 10 events where selected in data. In the  $\mu X$  channel, 11 events were selected with a calculated efficiency of  $(51.2 \pm 6.3)\%$  for  $e\mu\nu\nu$  production. For Standard Model values of the couplings,  $8.3 \pm 1.0$  single electron events were expected, comprising 4.48 events from  $ee\nu\nu$  production, 0.30 events from  $e\mu\nu\nu$ , 0.53 events from  $e\tau\nu\nu$  with the  $\tau$  decay products unseen, 0.15 events from the same final state but with an electron or positron from the  $\tau$  decay observed in the detector, and 2.80 events from the reaction  $e^+e^- \rightarrow e^+e^-\gamma(\gamma)$  with one electron (or positron) and the final state photon(s) unobserved. In the single muon channel,  $10.1 \pm 1.7$  events were expected for Standard Model values of the couplings, comprising 4.19 events from  $e\mu\nu\nu$  production, 2.41 events from  $e^+e^-\mu^+\mu^-$  production, 0.31 events from  $e\tau\nu\nu$ , 0.64 events from  $\mu\mu\nu\nu$ , 0.42 events

from  $\mu\tau\nu\nu$ , and 2.07 and 0.03 events from  $\mu\mu\gamma$  and  $\tau\tau\gamma$  production respectively. All of these contributions were estimated from simulated samples in which one final state lepton was emitted at less than  $11^\circ$ , and hence went undetected, or, if produced at larger angle, failed the reconstruction procedure. All the contributing channels except the Bhabha and Compton backgrounds in the  $eX$  final state and the  $\mu\mu\gamma$  and  $\tau\tau\gamma$  backgrounds in the  $\mu X$  channel have a dependence on trilinear gauge boson couplings in their production, and this was taken into account in the subsequent analysis.

### Selection of events in the $jjX$ topology:

Events were selected as candidates for the  $jjX$  topology, in which a lepton is presumed lost in the beam pipe and a neutrino is assumed to be produced, if they had total measured transverse momentum greater than  $20 \text{ GeV}/c$  and invariant mass of detected particles between  $45$  and  $90 \text{ GeV}/c^2$ . The detected particles were clustered into jets using LUCLUS with  $d_{join} = 6.5 \text{ GeV}/c$ , and events were accepted if they had two or three reconstructed jets. Surviving events were then forced into a 2-jet configuration.

Events from the  $WW$  final state with one  $W$  decaying leptonically were suppressed by rejecting events with identified final state leptons ( $e$  or  $\mu$ ) of energy exceeding  $12 \text{ GeV}$ . In order to suppress the contribution from the  $q\bar{q}\gamma$  final state, events were rejected if the angle between the planes containing each jet direction and the beam direction was less than  $20^\circ$ . In addition, events were rejected if the direction of either reconstructed jet lay within  $20^\circ$  of the beam direction, if any charged or neutral track of momentum exceeding  $1 \text{ GeV}/c$  was reconstructed within a cone of angle  $30^\circ$  about the direction of the missing momentum, or if there was a signal in the hermiticity detectors in a cone of angle  $50^\circ$  about the direction of the missing momentum.

Applying these criteria to fully simulated events, an efficiency of  $(43.7 \pm 1.5)\%$  was calculated; in the data 64 events were selected. For Standard Model values of the couplings, a total of  $60.3 \pm 0.8$  events are expected, comprising 17.0 events from the  $q\bar{q}e\nu$  final state with the electron or positron lost in the beam pipe, 5.13 events from  $q\bar{q}e\nu$  with the electron or positron elsewhere in the detector, 21.98 events from  $q\bar{q}\tau\nu$ , 8.10 events from  $q\bar{q}\mu\nu$ , 3.89 events from  $q\bar{q}\nu\nu$ , 4.00 events from  $q\bar{q}\gamma$  production, and 0.2 events from  $\gamma\gamma$  interactions. All the processes contributing to the selected sample except  $q\bar{q}\gamma$  production and two-photon interactions include diagrams with trilinear gauge couplings, and this was taken into account in the subsequent analysis.

### Selection of events in the $\gamma X$ topology:

The production of the single photon final state,  $\gamma X$ , via a  $WW\gamma$  vertex proceeds through the fusion diagram shown in figure 1c, while the dominant process giving rise to this final state,  $e^+e^- \rightarrow Z\gamma$ , with  $Z \rightarrow \nu\bar{\nu}$ , involves bremsstrahlung diagrams. The sensitivity of the  $\gamma X$  final states to anomalous  $WW\gamma$  couplings is therefore greatest when the photon is emitted at high polar angle. Events were selected if they had a single shower in the barrel electromagnetic calorimeter, with  $45^\circ < \theta_\gamma < 135^\circ$  and  $E_\gamma > 6 \text{ GeV}$ , where  $\theta_\gamma$  and  $E_\gamma$  are the polar angle and energy, respectively, of the reconstructed photon. It was also required that no electromagnetic showers were present in the forward electromagnetic calorimeters, and a second shower in the barrel calorimeter was accepted only if it was within  $20^\circ$  of the first one. Cosmic ray events were suppressed by requiring any signal in the hadronic calorimeter to be in the same angular region as the signal in the electro-

magnetic calorimeter and the electromagnetic shower to point towards the beam collision point [22]. Using these criteria, 145 events were selected from data corresponding to an integrated luminosity of  $155 \text{ pb}^{-1}$ . The Standard Model expectation is  $157.7 \pm 3.7$  events. Values for the triple gauge boson couplings were fitted in the region  $E_\gamma > 50 \text{ GeV}$ , which contained 59% of the events. In this region, an overall selection efficiency of  $(54 \pm 4)\%$  was estimated, with negligible background contamination.

### 3 Methods used to determine the couplings

The analysis procedures applied are similar to those used in our previously reported analysis of data at 183 GeV [2], though somewhat different applications of the method of Optimal Observables were used in the analyses of the  $jj\ell\nu$  and  $jjjj$  final states.

#### Optimal Observable Analysis of $jj\ell\nu$ and $jjjj$ channels

Data in both the  $jj\ell\nu$  and  $jjjj$  channels were analyzed using methods based on that of Optimal Observables [23]. The methods exploit the fact that the differential cross-section,  $d\sigma/d\vec{V}$ , where  $\vec{V}$  represents the phase space variables, is quadratic in the trilinear gauge coupling parameters:

$$\frac{d\sigma(\vec{V}, \vec{\lambda})}{d\vec{V}} = c_0(\vec{V}) + \sum_i c_1^i(\vec{V}) \cdot \lambda_i + \sum_{i \leq j} c_2^{ij}(\vec{V}) \cdot \lambda_i \cdot \lambda_j, \quad (1)$$

where the sums in  $i, j$  are over the set  $\vec{\lambda} = \{\lambda_1, \dots, \lambda_n\}$  of parameters under consideration. It has been shown that the “Optimal Variables”  $c_1^i(\vec{V})/c_0(\vec{V})$  and  $c_2^{ij}(\vec{V})/c_0(\vec{V})$ , approximated for real data by using the reconstructed phase space variables  $\vec{\Omega}$  as arguments of the  $c_1^i$  and  $c_2^{ij}$ , have the same estimating efficiency as can be obtained in unbinned likelihood fits of parameters  $\lambda_i$  to the data [24].

In the determination of a single parameter  $\lambda$ , the joint distribution of the quantities  $c_1(\vec{\Omega})/c_0(\vec{\Omega})$  and  $c_2(\vec{\Omega})/c_0(\vec{\Omega})$  was compared with the expected distribution, computed from events generated with EXCALIBUR and passed through the full detector simulation. An extended maximum likelihood fit, combining the information coming from the shape of the Optimal Variables and from the cross-section, has been carried out. At each stage the simulated data, which had been generated at a few values of the couplings, have been reweighted [25] to the required value of  $\lambda$  using the matrix element calculation of the ERATO generator [8]. In the case of events in the  $jj\ell\nu$  topology, the binning in these two variables was made using a multidimensional clustering technique, described in detail in [26]. This is an economical binning method in which the  $n_d$  real data points are used as seeds to divide the phase space into an equal number of multidimensional bins. Each simulated event is associated with the closest real event, resulting in an equiprobable division of the space of the Optimal Variables in which it is assumed that the best available knowledge of the probability density function is that of the real data points themselves.

The use of such a technique becomes of particular importance when simultaneous fits to two coupling parameters are performed. The number of Optimal Variables then increases to five:  $c_1^1/c_0$ ,  $c_1^2/c_0$ ,  $c_2^{11}/c_0$ ,  $c_2^{22}/c_0$  and  $c_2^{12}/c_0$ , and the use of equal sized bins in a space of this number of dimensions is impractical. For events in the  $jj\ell\nu$  topology, an

extended maximum likelihood fit was performed over the  $n_d$  bins for each pair of coupling parameters  $(\lambda_1, \lambda_2)$  using this method.

A somewhat different technique was used in 2-parameter fits to data in the  $jjjj$  topology. In this case, extended maximum likelihood fits were made to the binned joint distribution of only the first order terms  $c_1^1/c_0$  and  $c_1^2/c_0$  in (1), but an iterative procedure was used, at each stage expanding the expression for the differential distribution of the phase space variables  $\vec{V}$  about the values  $(\tilde{\lambda}_1, \tilde{\lambda}_2)$  obtained in the previous iteration:

$$\frac{d\sigma(\vec{V}, \lambda_1, \lambda_2)}{d\vec{V}} = c_0(\tilde{\lambda}_1, \tilde{\lambda}_2, \vec{V}) + c_1^1(\tilde{\lambda}_1, \tilde{\lambda}_2, \vec{V})(\lambda_1 - \tilde{\lambda}_1) + c_1^2(\tilde{\lambda}_1, \tilde{\lambda}_2, \vec{V})(\lambda_2 - \tilde{\lambda}_2) + \dots . \quad (2)$$

It has been shown in reference [24] that when this iterative procedure has converged sufficiently, the first order terms retain the whole sensitivity of the Optimal Variables to the coupling parameters  $\vec{\lambda}$ , the contribution from the higher order terms becoming negligible. In practice, this was achieved after about three or four iterations. As an example, figure 2 shows the distribution of  $c_1^{\Delta g_1^Z}(\vec{\Omega})/c_0(\vec{\Omega})$  for data and for the results of the fit described in the next section.

### Cross-check Analysis of $jj\ell\nu$ and $jjjj$ channels

In both the  $jj\ell\nu$  and  $jjjj$  channels, an additional analysis was performed using more directly measured kinematic variables in order to corroborate results obtained from the methods described above.

In the  $jj\ell\nu$  topology, a binned maximum likelihood fit was made to the joint distribution in  $\cos\theta_W$ , the  $W^-$  production angle, and  $\cos\theta_\ell$ , the polar angle of the produced lepton with respect to the incoming  $e^\pm$  of the same sign. In this study, somewhat looser criteria were imposed in the selection of the events, giving a total sample of 885 semileptonic events, with estimated efficiencies of  $(83.6 \pm 0.2)\%$ ,  $(70.9 \pm 0.3)\%$  and  $(47.9 \pm 0.4)\%$  for muon, electron and tau events, respectively, and an estimated background contamination of 1.0 pb. A 4-constraint kinematic fit was then applied to the events, requiring conservation of four-momentum, and the variables  $\cos\theta_W$  and  $\cos\theta_\ell$  computed from the fitted four-vectors. The expected number of events in each bin was estimated using events generated with PYTHIA corresponding to the reaction  $e^+e^- \rightarrow W^+W^-$  and passed through the full detector simulation procedure. Again, a reweighting technique was used to determine the expected number of events for given values of the coupling parameters. The distributions of  $\cos\theta_W$  and  $\cos\theta_\ell$  for real and simulated data are shown in figure 3.

In the  $jjjj$  topology, the second analysis involved a binned extended maximum likelihood fit to the production angular distribution. Events were selected by constructing a probability function from the distributions of eleven kinematic variables, namely: the value of  $d_{join}$  in the LUCLUS algorithm when four rather than three natural jets are reconstructed, the sphericity, the angle between the two most energetic jets, the minimal multiplicity in a jet, the second Fox-Wolfram moment, the  $D$  variable (defined above),  $s'$  (defined above), the fitted  $W$  masses, the product of the energy ratios of the two jets in the two reconstructed dijets, the minimal transverse momentum with respect to the beam axis of the 15 most energetic tracks in the event, and the transverse momentum of the jet pair obtained by forcing the reconstruction of exactly two jets. Using this procedure, a sample of 1331 events was selected with estimated efficiency of  $(86.6 \pm 0.2)\%$ .

and purity of  $(74.4 \pm 0.4)\%$ . As in the case of the optimal observable analysis of this channel described above, momentum-weighted jet charges were then calculated to try to distinguish the  $W^+$  decay products from those of the  $W^-$ . An angular variable  $x_g = \cos \theta_W (P_{W^-}(\Delta Q) - P_{W^+}(\Delta Q))$ , was constructed from the cosine of the  $W$  production angle and the difference in probability of a dijet to be coming from a  $W^-$  or  $W^+$  decay. The experimental distribution of  $x_g$  was compared with predictions obtained from events generated with PYTHIA, passed through the full detector simulation procedure, and reweighted in the fit for given values of the coupling parameters.

### Analysis of $\ell X$ , $jjX$ and $\gamma X$ channels

Data in the topologies  $\ell X$  and  $jjX$  were analysed using maximum likelihood fits to the observed total numbers of events selected, while the  $\gamma X$  data were fitted using a binned extended maximum likelihood fit to the distribution of the reconstructed photon energy,  $E_\gamma$ , in the region  $E_\gamma > 50$  GeV, which has the maximum sensitivity to anomalous triple gauge boson couplings.

## 4 Results

The preliminary results obtained for the triple gauge boson couplings from the data in each of the final states and using the methods discussed above are shown in table 1, together with their statistical and systematic errors (see below). The results from all topologies are combined with those previously analysed by DELPHI at 183 GeV and reported in reference [2] to give the values of the coupling parameters, their 1 s.d. errors and the 95% confidence limits shown in table 2. In the combination, which is done by adding the individual likelihood functions, the results in the  $jj\ell\nu$  and  $jjjj$  topologies from the methods based on Optimal Observables were used, as these use all the available kinematic information and hence are expected to have the greatest precision. In the fit to each coupling parameter, the values of the other parameters were held at zero, their Standard Model values. The results of fits in which two of the couplings  $\Delta g_1^Z$ ,  $\Delta\kappa_\gamma$  and  $\lambda_\gamma$  were allowed to vary are shown in figure 4a-c. In no case is any deviation seen from the Standard Model prediction of zero for the couplings determined.

The results shown in figure 4c can be transformed to produce estimates for the magnetic dipole moment,  $\mu_W$ , and the electric quadrupole moment,  $q_W$ , of the  $W$  boson using the relations

$$\mu_W = \frac{e}{2m_W} (g_1^\gamma + \kappa_\gamma + \lambda_\gamma) \quad \text{and} \quad (3)$$

$$q_W = -\frac{e}{m_W^2} (\kappa_\gamma - \lambda_\gamma). \quad (4)$$

The resulting two-parameter fit gives the values

$$\begin{aligned} \mu_W \cdot \frac{2m_W}{e} &= 2.22^{+0.20}_{-0.19} \quad \text{and} \\ q_W \cdot \frac{m_W^2}{e} &= -1.18^{+0.27}_{-0.26} \end{aligned}$$

with the confidence level contours shown in figure 4d. In the derivation of the result for  $\mu_W$ , the value of  $g_1^\gamma$ , the  $WW\gamma$  charge coupling, has been assumed to be unity, as required by electromagnetic gauge invariance. The quantity  $(g - 2)_W$ , derived from the definition of the gyromagnetic ratio of a particle of spin  $\vec{s}$ , charge  $Q$  and mass  $m$ ,  $\vec{\mu} = g\vec{s}\frac{Q}{2m}$ , is, therefore, measured to be  $(g - 2)_W = 0.22^{+0.22}_{-0.20}$ . All values are preliminary.

### Systematic uncertainties:

The systematic errors shown in table 1 and included in the results shown in table 2 contain contributions from various sources. Table 3 lists the dominant sources of systematic uncertainties for each of the analyses used in the combination. A distinction between systematic errors affecting more than one channel, and effects specific to only one channel is made in the combination of the different channels. The list of common systematic effects and the procedure for their combination is given later in this section.

In the  $jj\ell\nu$  channel, the dominant effect for  $\Delta g_1^Z$  and  $\lambda_\gamma$  arises from the uncertainty in the background contamination, which is taken to be 10%. For  $\Delta\kappa_\gamma$ , the event reconstruction effects give the largest single contribution. Comparisons between  $Z$  data and fully simulated events were used to estimate uncertainties of jet and lepton energies and of their angular distributions. These uncertainties were then used to derive an additional smearing for a sample of simulated events, which was then also fitted to the data. The difference arising from fitting this sample and the standard sample is quoted as the event reconstruction uncertainty. A further effect considered was the possibility of misassignment of the lepton charge. This was again studied in  $Z$  data, where the fraction of events with misidentified lepton charge was found to be 0.3%. The corresponding systematic effect was calculated by fitting to a simulated sample of  $jj\ell\nu$  data with 0.3% of the events randomly assigned the wrong lepton charge. Also included are the effects of limited Monte Carlo statistics in the evaluation of signal efficiencies.

In the  $jjjj$  channel, the dominant effect for  $\Delta g_1^Z$  comes from different centre-of-mass energies between data and simulation; it was evaluated by comparing samples generated at 188 and 190 GeV and is labelled ‘beam energy’ in table 3. For  $\lambda_\gamma$ , the largest source is due to uncertainties in the jet hadronisation models used. It was estimated by comparing data sets in which the JETSET and HERWIG [28] fragmentation models were applied to a common set of generated events. The effects of colour reconnection following the SK1 model [29] were investigated by performing a similar comparison between a sample with maximal reconnection probability and the standard unconnected set of JETSET events. Also studied was again the uncertainty in the background contamination (5%).

In the single  $W$  channels  $\ell X$  and  $jjX$ , the dominant source of systematic errors is the uncertainty in the efficiency estimation, which is an effect of the limited amount of simulated events available. This also affects the background estimation.

In the  $\gamma X$  channel, systematic effects play only a minor role. The main systematic contribution originates from the uncertainty in the energy reconstruction of the barrel electromagnetic calorimeter.

As in our previous analysis [2], the combined results shown in table 2 include the independent systematic errors from each channel. Systematic effects common to more than one channel, such as the theoretical uncertainty in the  $WW$  cross-section, the uncertainty in the  $W$  mass, the luminosity measurement and in the LEP beam energy are taken into account separately. The most interesting effect among these correlated sys-

tematics is the uncertainty in the  $WW$  cross-section calculation. To estimate this effect, the cross-section was varied by its theoretical error of 2%. The effect of this variation is quite small, particularly in the  $jj\ell\nu$  channel, which contains the highest sensitivity to the couplings studied. This is reassuring given that a more precise evaluation of the cross-section is now available [27], which gives a value around 2% lower than currently assumed. As this new cross-section calculation is not yet implemented in our event generators, we use the old calculations and quote a systematic error which covers the difference between the two cross-section values. The common effects are evaluated individually for each final state and then added with weights derived from the statistical precision of the individual channels with respect to each coupling.

## 5 Conclusions

Values for the  $WWV$  couplings  $\Delta g_1^Z$ ,  $\Delta\kappa_\gamma$  and  $\lambda_\gamma$  have been derived from an analysis of DELPHI data at 189 GeV. The results have been combined with previously published values from DELPHI data at lower energies, giving an overall improvement in precision by a factor of about two over that of the 183 GeV data [2]. The results of the 2-parameter fit to the couplings  $\Delta\kappa_\gamma$  and  $\lambda_\gamma$  have been used to derive values for the magnetic dipole and electric quadrupole moments of the  $W$  and for the  $W$  gyromagnetic ratio.

There is no evidence for deviations from Standard Model predictions in any of the results obtained.

## References

- [1] DELPHI Collaboration, P. Abreu *et al.*, Phys. Lett. **B423** (1998) 194.
- [2] DELPHI Collaboration, P. Abreu *et al.*, Phys. Lett. **B459** (1999) 382.
- [3] K. Hagiwara, R. Peccei, D. Zeppenfeld and K. Hikasa, Nucl. Phys. **B282** (1987) 253.
- [4] G. Gounaris, J.-L. Kneur and D. Zeppenfeld, in *Physics at LEP2*, eds. G. Altarelli, T. Sjöstrand and F. Zwirner, CERN 96-01 Vol.1, 525 (1996).
- [5] DELPHI Collaboration, P. Aarnio *et al.*, Nucl. Inst. Meth. **A303** (1991) 233,  
DELPHI Collaboration, P. Abreu *et al.*, Nucl. Inst. Meth. **A378** (1996) 57,  
DELPHI Collaboration, P. Abreu *et al.*, “Proposal for the upgrade of DELPHI in the forward region”, DELPHI internal note 92-142 GEN 135.
- [6] DELPHI Collaboration, P. Abreu *et al.*, E. Phys. J. **C2** (1998) 581.
- [7] F.A. Berends, R. Kleiss and R. Pittau, *EXCALIBUR*, in *Physics at LEP2*, eds. G. Altarelli, T. Sjöstrand and F. Zwirner, CERN 96-01 Vol.2, 23 (1996).
- [8] C.G. Papadopoulos, Comp. Phys. Comm. **101** (1997) 183.
- [9] O. Yushchenko, *DELTGC: A program for four-fermion calculations*, DELPHI note DELPHI 99-4 PHYS 816 (1999).

- [10] J. Fujimoto *et al.*, *GRC4F*, in *Physics at LEP2*, eds. G. Altarelli, T. Sjöstrand and F. Zwirner, CERN 96-01 Vol.2, 23 (1996).
- [11] G. Montagna *et al.* Nucl. Phys. **B452** (1995) 161.
- [12] T. Sjöstrand, *PYTHIA 5.7 / JETSET 7.4*, CERN-TH.7112/93 (1993).
- [13] DELPHI Collaboration, P. Abreu *et al.*, Z. Phys. **C73** (1996) 11.
- [14] T. Sjöstrand, *PYTHIA 5.719 / JETSET 7.4*, in *Physics at LEP2*, eds. G. Altarelli, T. Sjöstrand and F. Zwirner, CERN 96-01 Vol.2, 41 (1996).
- [15] S. Jadach, B.F.L Ward and Z. Was, Comp. Phys. Comm. **79** (1994) 503.
- [16] S. Jadach, W. Placzek, B.F.L. Ward, Phys. Lett. **B390** (1997) 298.
- [17] D. Karlen, Nucl. Phys. **B289** (1987) 23.
- [18] F.A. Berends, P.H. Daverveldt and R. Kleiss, Comp. Phys. Comm. **40** (1980) 271, 285 and 309.
- [19] S. Nova, S. Olchevski and T. Todorov, in *Physics at LEP2*, eds. G. Altarelli, T. Sjöstrand and F. Zwirner, CERN 96-01 Vol.2, 224 (1996).
- [20] P. Abreu *et al.*, Nucl. Inst. Meth. **A427** (1999) 487.
- [21] ALEPH Collaboration, R. Barate *et al.*, Phys. Lett. **B422** (1998) 369.
- [22] DELPHI Collaboration, P. Abreu *et al.*, EP 2000-021, accepted by E.Phys. J **C**, (2000).
- [23] M. Diehl and O. Nachtmann, Z. Phys. **C62** (1994) 397.
- [24] G.K. Fanourakis, D. Fassouliotis and S.E. Tzamarias, Nucl. Inst. Meth. **A414** (1998) 399;  
G.K. Fanourakis, D. Fassouliotis, A. Leisos, N. Mastroiannopoulos and S.E. Tzamarias, Nucl. Inst. Meth. **A430** (1999) 474.
- [25] G.K. Fanourakis, D. Fassouliotis and S.E. Tzamarias, Nucl. Inst. Meth. **A412** (1998) 465.
- [26] G.K. Fanourakis, D. Fassouliotis, A. Leisos, N. Mastroiannopoulos and S.E. Tzamarias, Nucl. Inst. Meth. **A430** (1999) 455.
- [27] M. Grünwald, G. Passarino, *et al.*, Four-Fermion Production in Electron-Positron Collisions, hep-ph/0005309, (2000).
- [28] G. Abbiendi, I.G. Knowles, G. Marchesini, M.H. Seymour, L. Stanco, B.R. Webber, Computer Phys. Commun. **67** (1992) 465.
- [29] T.Sjöstrand and V.A. Khoze, Zeit. Phys. **C62** (1994) 281,  
T.Sjöstrand and V.A. Khoze, Phys. Rev. Lett. **72** (1994) 28.

	$\Delta g_1^Z$	$\Delta \kappa_\gamma$	$\lambda_\gamma$
$jj\ell\nu$ (Optimal Variables)	$0.00^{+0.08}_{-0.08} \pm 0.02$	$0.28^{+0.35}_{-0.28} \pm 0.10$	$0.06^{+0.09}_{-0.09} \pm 0.02$
$jj\ell\nu$ ( $\cos \theta_W$ , $\cos \theta_\ell$ )	$-0.04^{+0.12}_{-0.11} \pm 0.03$	$0.00^{+0.48}_{-0.28} \pm 0.10$	$0.01^{+0.15}_{-0.13} \pm 0.03$
$jjjj$ (Optimal Variables)	$-0.09^{+0.14}_{-0.12} \pm 0.07$	$0.12^{+0.54}_{-0.31} \pm 0.24$	$0.01^{+0.17}_{-0.15} \pm 0.05$
$jjjj$ ( $\cos \theta_W$ )	$-0.07^{+0.17}_{-0.13} \pm 0.06$	$0.06^{+0.57}_{-0.31} \pm 0.23$	$-0.05^{+0.19}_{-0.15} \pm 0.06$
$\ell X$	$-0.45^{+1.35}_{-0.38} \pm 0.21$	$0.23^{+0.27}_{-0.34} \pm 0.19$	$0.48^{+0.33}_{-1.27} \pm 0.21$
$jjX$	$-0.43^{+1.31}_{-0.39} \pm 0.25$	$0.19^{+0.34}_{-0.57} \pm 0.11$	$0.42^{+0.36}_{-1.20} \pm 0.15$
$\gamma X$	—	$0.70^{+0.77}_{-0.99} \pm 0.03$	$0.65^{+1.03}_{-1.79} \pm 0.09$

Table 1: Fitted values of  $WWV$  couplings from DELPHI data at 189 GeV using the methods described in the text. The first error given for each value is the 1 s.d. statistical error; the second is the systematic error. In the fits to each coupling parameter, the other couplings were set to their Standard Model values. All values are preliminary.

Coupling parameter	Value	95% confidence interval
$\Delta g_1^Z$	$-0.02^{+0.07}_{-0.07} \pm 0.01$	$-0.16, 0.13$
$\Delta \kappa_\gamma$	$0.25^{+0.21}_{-0.20} \pm 0.06$	$-0.13, 0.68$
$\lambda_\gamma$	$0.05^{+0.09}_{-0.09} \pm 0.01$	$-0.11, 0.23$

Table 2: Values of triple gauge boson couplings combining DELPHI data from various topologies and energies, as described in the text. The second column shows the value of each coupling corresponding to the minimum of the combined negative log-likelihood distribution and its 1 s.d. errors. The first error quoted is the combined statistical and uncorrelated systematic error, the second is the total common systematic (see text). The third column shows the 95% confidence intervals on the parameter values, computed by stepping up 2.0 units from the minimum of the likelihood curve. In the fits to each coupling parameter, the other two couplings were set to their Standard Model values. All values are preliminary.

Channel	Source & Method	$\Delta g_1^Z$	$\Delta \kappa_\gamma$	$\lambda_\gamma$
$jj\ell\nu$	Background estimation	$\pm 0.013$	$\pm 0.058$	$\pm 0.014$
	Signal cross-section	$\pm 0.002$	$\pm 0.018$	$\pm 0.002$
	Lepton charge assignment	$\pm 0.005$	$\pm 0.035$	$\pm 0.009$
	Signal MC statistics	$\pm 0.005$	$\pm 0.017$	$\pm 0.006$
	Event reconstruction	$\pm 0.005$	$\pm 0.064$	$\pm 0.006$
	Total $jj\ell\nu$ systematic	$\pm 0.017$	$\pm 0.097$	$\pm 0.019$
$jjjj$	Background estimation	$\pm 0.02$	$\pm 0.05$	$\pm 0.01$
	Signal cross-section	$\pm 0.02$	$\pm 0.13$	$\pm 0.01$
	Colour reconnection	$\pm 0.03$	$\pm 0.07$	$\pm 0.01$
	Fragmentation	$\pm 0.01$	$\pm 0.11$	$\pm 0.03$
	Beam energy	$\pm 0.05$	$\pm 0.11$	$\pm 0.02$
	Total $jjjj$ systematic	$\pm 0.07$	$\pm 0.24$	$\pm 0.05$
$\ell X$	Background estimation	$\pm 0.13$	$\pm 0.13$	$\pm 0.12$
	Signal cross-section	$\pm 0.08$	$\pm 0.05$	$\pm 0.07$
	Efficiency estimation	$\pm 0.15$	$\pm 0.13$	$\pm 0.16$
	Total $\ell X$ systematic	$\pm 0.21$	$\pm 0.19$	$\pm 0.21$
$jjX$	Background estimation	$\pm 0.03$	$\pm 0.02$	$\pm 0.03$
	Signal cross-section	$\pm 0.08$	$\pm 0.06$	$\pm 0.08$
	Efficiency estimation	$\pm 0.23$	$\pm 0.09$	$\pm 0.12$
	Total $jjX$ systematic	$\pm 0.25$	$\pm 0.11$	$\pm 0.15$
$\gamma X$	Energy reconstruction	—	$\pm 0.03$	$\pm 0.09$
	Signal cross-section	—	$\pm 0.01$	$\pm 0.01$
	Efficiency estimation	—	$\pm 0.01$	$\pm 0.01$
	Total $\gamma X$ systematic	—	$\pm 0.03$	$\pm 0.09$

Table 3: Main systematic contributions in each analysed channel.

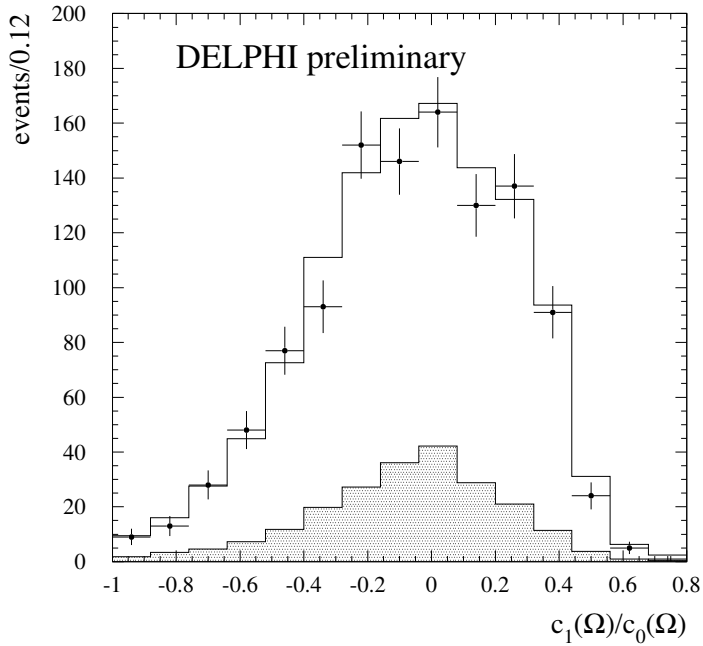


Figure 2: Distribution of the optimal variable  $c_1^{\Delta g_1^Z}(\vec{\Omega})/c_0(\vec{\Omega})$  (defined in the text) for the coupling  $\Delta g_1^Z$  in the  $jjjj$  channel from DELPHI data at 189 GeV. The points represent the data and the histogram shows the distribution expected for the fitted value of  $\Delta g_1^Z$  (see table 1). The shaded area is the estimated background contribution.

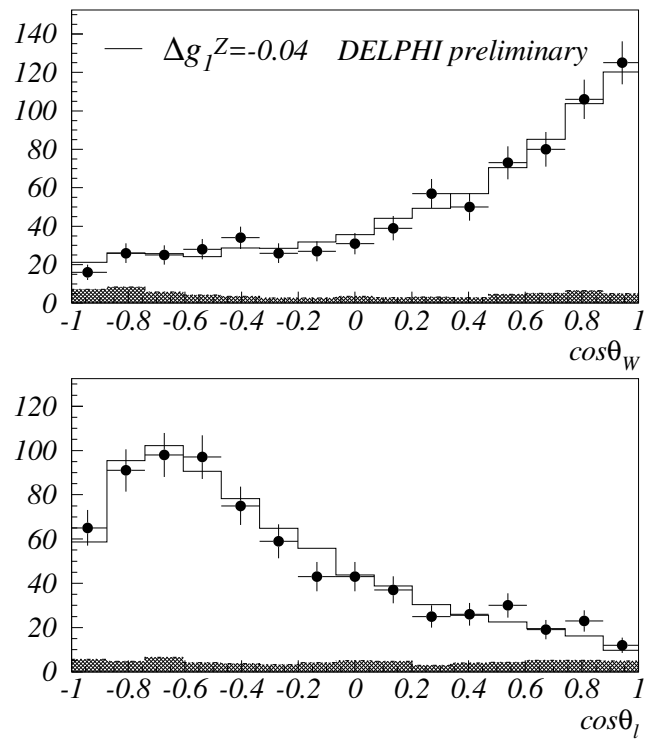


Figure 3: Distributions in  $\cos \theta_W$  and  $\cos \theta_\ell$  for  $jj\ell\nu$  events ( $\ell \equiv e, \mu, \tau$ ) for DELPHI data, shown as dots, at 189 GeV. The histogram shows the distribution expected for the fitted value of  $\Delta g_1^Z$  (see table 1). The shaded area is the estimated background contribution.

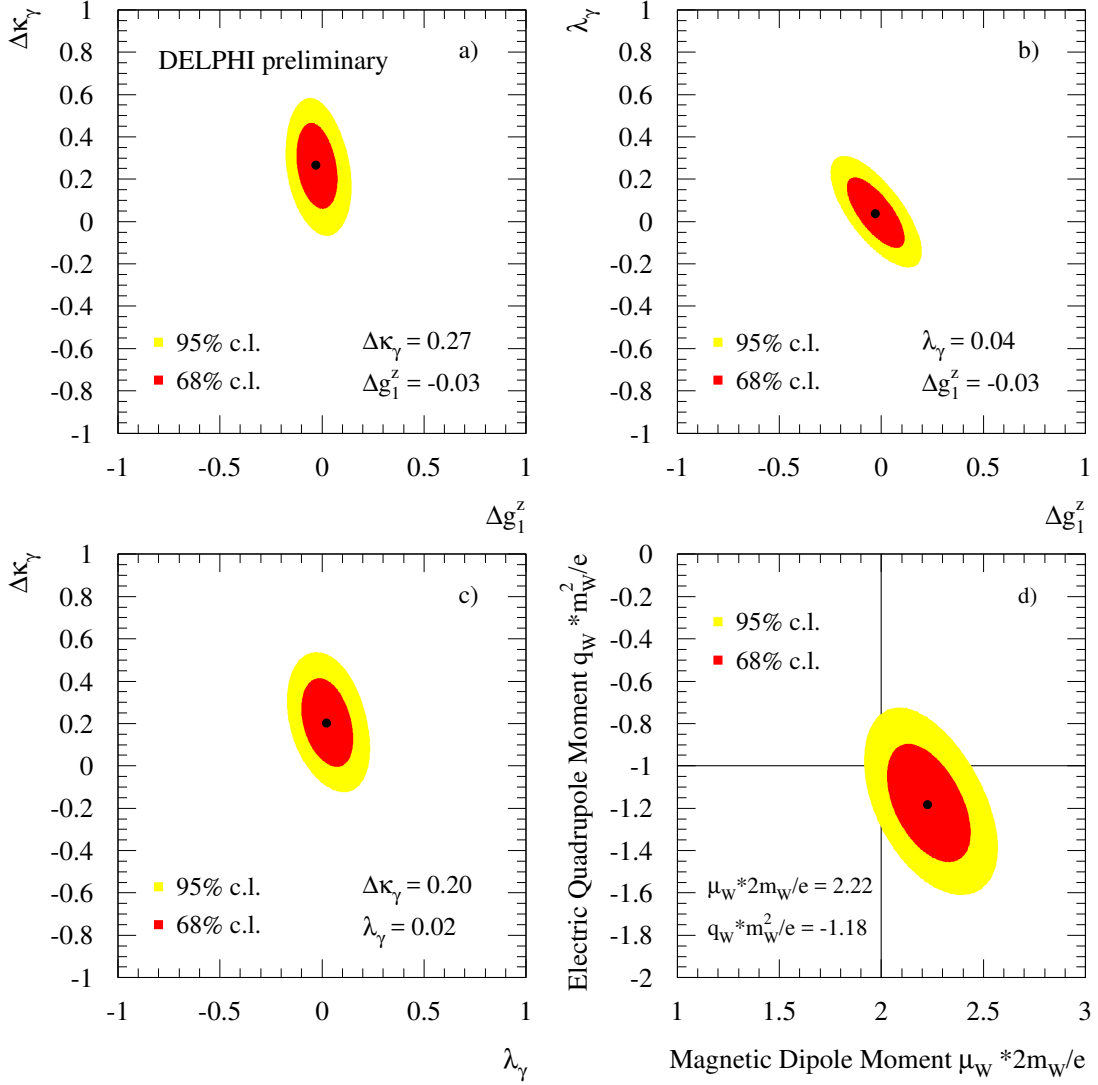


Figure 4: Results of fits in the planes of the parameters a)  $(\Delta\kappa_\gamma, \Delta g_1^Z)$ , b)  $(\lambda_\gamma, \Delta g_1^Z)$ , c)  $(\Delta\kappa_\gamma, \lambda_\gamma)$  and d)  $(\mu_W, q_W)$  using data from the final states listed in table 1 combined with DELPHI results at lower energy [2]. In the combination, the analyses of the  $jj\ell\nu$  and  $jjjj$  final states based on Optimal Observable techniques were used. In each case the third parameter was fixed at its Standard Model value. The values maximizing the likelihood function and the regions accepted at the 68% and 95% confidence levels are shown. The confidence intervals are computed as the contours where the value of the likelihood function is increased by 1.15 units (68% c.l.) and 3.0 units (95% c.l.) respectively from the minimum.